Draft version July 12, 2018
Typeset using LaTeX **twocolumn** style in AASTeX61

# ASTROPHYSICAL S-FACTORS, THERMONUCLEAR RATES, AND ELECTRON SCREENING POTENTIAL FOR THE $^3$He(d,p)$^4$He BIG BANG REACTION VIA A HIERARCHICAL BAYESIAN MODEL

Rafael S. de Souza,[1] Christian Iliadis,[1] and Alain Coc[2]

[1] *Department of Physics & Astronomy, University of North Carolina at Chapel Hill, NC 27599-3255, USA*
[2] *Centre de Sciences Nucléaires et de Sciences de la Matière, Univ. Paris-Sud, CNRS/IN2P3, Université Paris-Saclay, Bâtiment, 104, F-91405 Orsay Campus, France*

(Received July 12, 2018)

Submitted to ApJ

## ABSTRACT

We developed a hierarchical Bayesian framework to estimate S-factors and thermonuclear rates for the $^3$He(d,p)$^4$He reaction, which impacts the primordial abundances of $^3$He and $^7$Li. The available data are evaluated and only those direct measurements are taken into account in our analysis for which we can estimate separate uncertainties for systematic and statistical effects. For the nuclear reaction model we adopt a single-level, two-channel approximation of R-matrix theory, suitably modified to take the effects of electron screening at lower energies into account. Apart from the usual resonance parameters (resonance location and partial widths for the incoming and outgoing reaction channel), we include for the first time the channel radii and boundary condition parameters in the model evaluation. Our new analysis of the $^3$He(d,p)$^4$He S-factor data results in improved estimates for the thermonuclear rates and associated uncertainties. This work represents the first nuclear rate evaluation using R-matrix theory embedded into a hierarchical Bayesian framework, properly accounting for all known sources of uncertainty. Therefore, it provides a test bed for future studies of more complex reactions.

*Keywords:* nuclear reactions, nucleosynthesis, methods: statistical

Corresponding author: Rafael S. de Souza
Corresponding author: Christian Iliadis
drsouza@ad.unc.edu,iliadis@unc.edu

## 1. INTRODUCTION

The big-bang theory rests on three observational pillars: big-bang nucleosynthesis (BBN; Gamow 1948; Cyburt et al. 2016), the cosmic expansion (Riess et al. 1998; Peebles & Ratra 2003), and the cosmic microwave background radiation (Spergel et al. 2007; Planck Collaboration et al. 2016). The BBN takes place during the first 20 minutes after the big bang, at temperatures and densities near 1 GK and $10^{-5}$ g/cm$^3$, and is responsible for the production of the light nuclides, which play a major role in the subsequent history of cosmic evolution.

Primordial nucleosynthesis provides a sensitive test of the big bang model if the uncertainties in the predicted abundances can be reduced to the uncertainty level of the observed values. The uncertainties for the observed primordial abundances of $^4$He, $^2$H (or d), and $^7$Li have been greatly reduced in recent years and amount to 1.6%, 1.6%, and 20%, respectively (Coc et al. 2015). For the observed primordial $^3$He abundance, only an upper limit[1] is available ($^3$He/H $\leq 1.3 \times 10^{-5}$; Bania et al. 2002). At present, the uncertainties in the predicted abundances of $^4$He, $^2$H (or d), $^3$He, and $^7$Li amount to 0.08%, 2.0%, 2.8%, and 4.6%, respectively (Coc et al. 2015). The primordial abundances predicted by the big bang model are in reasonable agreement with observations, as shown in Figure 1, except for the $^7$Li/H ratio, where the predicted value (Cyburt et al. 2016) exceeds the observed one (Sbordone et al. 2010) by a factor of $\approx$ 3. This long-standing "lithium problem" has not found a satisfactory solution yet.

Twelve nuclear processes of interest take place during big bang nucleosynthesis, (Figure 2). Among these are the weak interactions that transform neutrons into protons, and vice versa, and the p(n,$\gamma$)d reaction whose cross section can be calculated precisely using effective field theories (Savage et al. 1999). The ten remaining reactions, d(p,$\gamma$)$^3$He, d(d,n)$^3$He, d(d,p)t, t(d,n)$^4$He, t($\alpha$,$\gamma$)$^7$Li, $^3$He(d,p)$^4$He, $^3$He(n,p)t, $^3$He($\alpha$,$\gamma$)$^7$Be, $^7$Li(p,$\alpha$)$^4$He, and $^7$Be(n,p)$^7$Li, have been measured directly in the laboratory at the energies of astrophysical interest. Nevertheless, the estimation of thermonuclear reaction rates from the measured cross section (or S-factor) data remains challenging. Results obtained using $\chi^2$ optimization are plagued by a number of problems, including the treatment of systematic uncertainties and the implicit assumption of normal likelihoods. Therefore, we have started a program to derive statistically sound BBN reaction rates using a hierarchical Bayesian model. Bayesian rates have recently been derived for d(p,$\gamma$)$^3$He, $^3$He($\alpha$,$\gamma$)$^7$Be (Iliadis et al. 2016), d(d,n)$^3$He, and d(d,p)$^3$H (Gómez Iñesta et al. 2017). These studies adopted the cross section energy dependence from the microscopic theory of nuclear reactions, while the absolute cross section normalization was found from a fit to the data within the Bayesian framework.

We report here the Bayesian reaction rates for the fifth big bang reaction, $^3$He(d,p)$^4$He. This reaction marginally impacts the primordial deuterium abundance, but sensitively influences the primordial abundances of $^3$He and $^7$Li (Coc & Vangioni 2010). Because of its low abundance, $^3$He has not been observed yet outside of our Galaxy. However, the next generation of large telescope facilities will likely enable the determination of the $^3$He/$^4$He ratio from observations of extragalactic metal-poor HII regions (Cooke 2015).

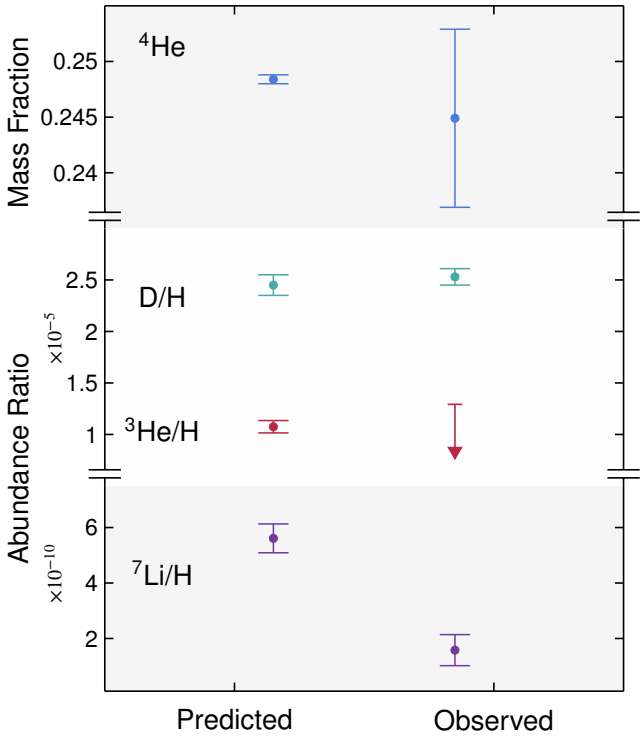


**Figure 1.** Predicted (left) versus observed (right) primordial abundances for the light nuclei: $^4$He, D, $^3$He and $^7$Li. For $^4$He the mass fraction is shown, while for the other species it is shown the number abundance ratios relative to hydrogen. The $2\sigma$ bars for the predicted abundances are from Coc et al. (2015), while the observed abundances are obtained from Aver et al. (2015) ($^4$He), Cooke et al. (2014) (D), and Sbordone et al. (2010) ($^7$Li). For the observed primordial $^3$He abundance only an upper limit is available (Bania et al. 2002), which we depict by a vertical arrow.

[1] Notice that the upper limit in Bania et al. 2002 is reported as "$(1.1\pm0.2)\times10^{-5}$" and, unfortunately, is frequently misinterpreted as an actual mean value with an error bar.

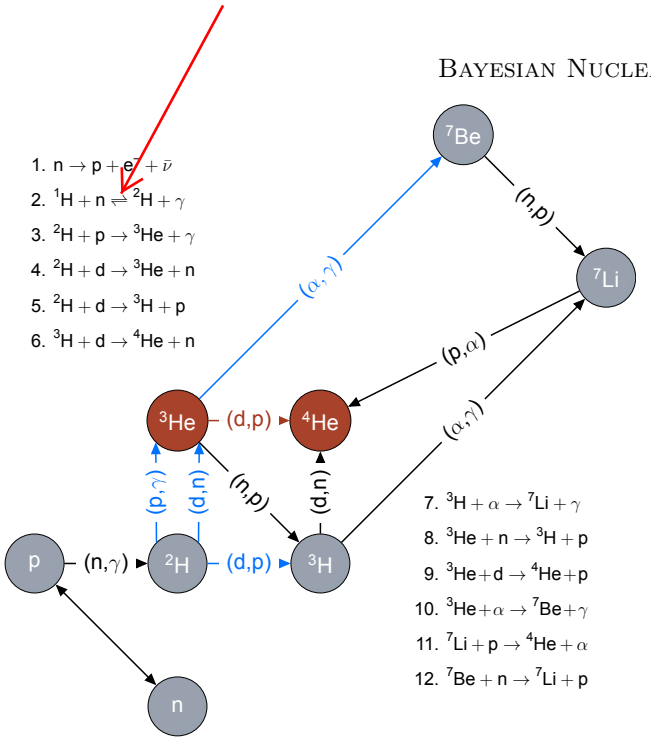


**Figure 2.** Nuclear reactions important for big bang nucleosynthesis. Reactions for which the rates have been obtained previously using Bayesian models are shown as blue arrows. The $^3$He(d,p)$^4$He reaction, which is subject of the present work, is shown in red.

Therefore, although a revised $^3$He(d,p)$^4$He reaction rate is unlikely to solve the $^7$Li problem, a more reliable rate is nevertheless desirable for improving the predicted BBN abundances.

The $^3$He(d,p)$^4$He reaction has been studied extensively during the past few decades, not only because of its importance to BBN, but also because its relevance to the understanding of the electron screening potential effects (e.g. La Cognata et al. 2005). At the lowest energies, the measured astrophysical S-factor shows a marked increase caused by electron screening effects. The data at those energies were used to derive the electron screening potential, but the results depended strongly on the data sets analyzed and the nuclear model applied.

To enable a robust treatment of different sources of uncertainties, we first perform a meta-analysis in the available cross section data and take only those experiments into account for which we can quantify the separate contributions of statistical and systematic effects to the total uncertainty. This leaves us with seven data sets to be analyzed. For the underlying nuclear model we assume a single-level, two-channel approximation of R-matrix theory. As will be discussed below, we introduce for the first time the channel radii and boundary conditions as parameters into the statistical model. Compared to previous works (Iliadis et al. 2016; Gómez Iñesta et al. 2017), the present Bayesian model is more complicated and, therefore, represents an important testbed for future studies of even more complex systems.

In Section 2, we summarize the reaction formalism. Our Bayesian model is discussed in Section 3, including likelihoods, model parameters, and priors. In Section 4, we present Bayesian S-factors and screening potentials. The thermonuclear reaction rates are presented in section 5. A summary and conclusions are given in Section 6. Appendix A lists the data we adopted in our analysis.

## 2. REACTION FORMALISM

Cross section (or S-factor) data for the $^3$He(d,p)$^4$He reaction have been fitted in the past using various assumptions, including polynomials (Krauss et al. 1987), a Padé expansion (Barbui et al. 2013), R-matrix expressions (Barker 2007), and hybrid models (Prati et al. 1994). See also Barker (2002) for a summary. Since we are mostly interested in the low-energy region where the s-wave contribution dominates the cross section, we follow Barker (1997) and describe the theoretical energy dependence of the cross section (or S-factor) using a one-level, two-channel R-matrix approximation, suitably modified to take electron screening at low energies into account.

The integrated cross section of the $^3$He(d,p)$^4$He reaction is given by

$$\sigma_{dp}(E) = \frac{\pi}{k_d^2}\frac{2J+1}{(2j_1+1)(2j_2+1)}\left|S_{dp}\right|^2, \qquad (1)$$

where $k_d$ and $E$ are the deuteron wave number and center-of-mass energy, respectively, J = 3/2 is the resonance spin, $j_1 = 1/2$ and $j_2 = 1$ are the ground-state spins of $^3$He and deuteron, respectively, and $S_{dp}$ is the scattering matrix element. The corresponding bare nucleus astrophysical S-factor of the $^3$He(d,p)$^4$He reaction, which is not affected by electron screening, is given by

$$S_{bare}(E) = Ee^{2\pi\eta}\sigma_{dp}(E), \qquad (2)$$

where $\eta$ is the Sommerfeld parameter. The scattering matrix element can be expressed as (Lane & Thomas 1958)

$$\left|S_{dp}\right|^2 = \frac{\Gamma_d\Gamma_p}{(E_0+\Delta-E)^2+(\Gamma/2)^2}, \qquad (3)$$

where $E_0$ represents the level eigenenergy. The partial widths of the $^3$He + d and $^4$He + p channels ($\Gamma_d$, $\Gamma_p$), the total width ($\Gamma$), and the level shift ($\Delta$) are given by

$$\Gamma = \sum_c \Gamma_c\ , \quad \Gamma_c = 2\gamma_c^2 P_c, \qquad (4)$$

$$\Delta = \sum_c \Delta_c \ , \quad \Delta_c = -\gamma_c^2 (S_c - B_c), \tag{5}$$

where $\gamma_c^2$ is the reduced width, and $B_c$ is the boundary condition parameter. The energy-dependent quantities $P_c$ and $S_c$ denote the penetration factor and shift factors, respectively, for channel $c$ (either d + $^3$He or p + $^4$He), which are computed from the Coulomb wave functions, $F_l$ and $G_l$, according to:

$$P_c = \frac{k_d a_c}{F_\ell^2 + G_\ell^2}, \qquad S_c = \frac{k_d a_c (F_\ell F'_\ell + G_\ell G'_\ell)}{F_\ell^2 + G_\ell^2}. \tag{6}$$

The Coulomb wave functions and their derivatives are evaluated at the channel radius, $a_c$; $\ell$ denotes the orbital angular momentum for a given channel.

The R-matrix channel radius is usually expressed as

$$a_c = r_0 \left( A_1^{1/3} + A_2^{1/3} \right), \tag{7}$$

where $A_1$ and $A_2$ are the mass numbers of the two interacting nuclei; $r_0$ denotes the radius parameter, with a value customarily chosen between 1 fm and 2 fm. For the $^3$He(d,p)$^4$He reaction, previous choices for the channel radii ranged between 3 fm and 6 fm (e.g., Barker 2002; Descouvemont et al. 2004). R-matrix parameters and cross sections derived from data have a well-known dependence on the channel radii, which arises from the truncation of the R-matrix to a restricted number of poles (i.e., a finite set of eigenenergies). The radius of a given channel has no rigorous physical meaning, except that the chosen values should exceed the sum of the radii of the colliding nuclei (e.g. Descouvemont & Baye 2010). We will discuss the impact of varying the channel radii on our derived S-factors in Section 4.

For a narrow resonance, the observed resonance energy, $E_r$, i.e., the peak of the observed cross section or S-factor, can be defined as:

$$E_0 + \Delta(E_r) - E_r = 0. \tag{8}$$

The boundary condition parameter is then chosen as:

$$B_c = S_c(E_r), \tag{9}$$

so that the level shift becomes zero at the observed resonance energy. This assumption, corresponding to setting the eigenenergy equal to the observed resonance energy in the data fitting ($E_r = E_0$), has been adopted in most previous studies (e.g. Barker 2007). However, it does not necessarily apply to broad resonances, where the maximum of the scattering matrix element, cross section, and S-factor peak at different energies. Indeed, for the low-energy $^3$He(d,p)$^4$He resonance, the total observed width is approximately equal to the observed resonance energy. We will investigate in Section 4 the impact of varying the boundary condition parameters on our results.

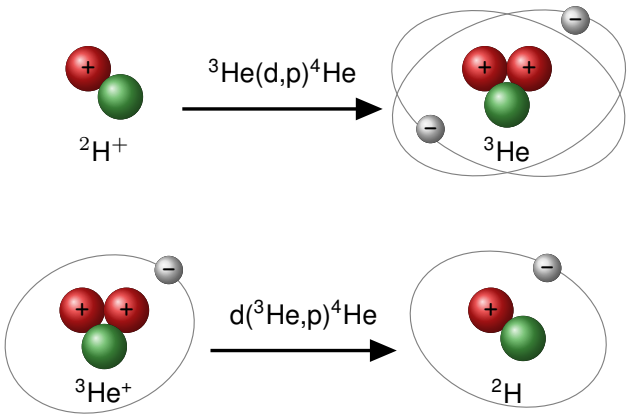


**Figure 3.** Illustration of the different configurations involved in the $^3$He(d,p)$^4$He and d($^3$He,p)$^4$He reactions. Top: Deuterium ion beam (with no atomic electron) incident on a neutral $^3$He target atom. Bottom: $^3$He ion (with one atomic electron) incident on a neutral deuterium target atom. The electron screening effect is of different magnitude in these two situations.

In laboratory experiments, electrons are usually bound to the interacting projectile and target nuclei. These electron clouds effectively reduce the Coulomb barrier and give rise to an increasing transmission probability. We perform the S-factor fit to the data using the expression (Assenbaum et al. 1987; Engstler et al. 1988):

$$S(E) \approx S_{bare}(E) e^{\pi\eta(U_e/E)}, \tag{10}$$

where $U_e$ is the energy-independent electron screening potential.

Notice that the measurement can be performed in two ways, depending on the identity of the projectile and target. The situation is shown in Figure 3. The notation $^3$He(d,p)$^4$He refers to a deuterium ion beam (without atomic electrons) directed onto a neutral $^3$He target, while d($^3$He,p)$^4$He refers to a $^3$He ion beam directed onto a neutral deuterium target. These two situations result in different electron screening potentials, $U_e$. The distinction is particularly important at center-of-mass energies below 50 keV, as will be shown below.

## 3. BAYESIAN MODEL

### 3.1. *General aspects*

Bayesian probability theory provides a mathematical framework to infer, from the measured data, the degree of plausibility of model parameters. (Jaynes & Bretthorst 2003). It allows to update a current state of

knowledge about a set of model parameters, $\theta$, in view of newly available information. The updated state of knowledge about $\theta$ is described by the posterior distribution, $p(\theta|y)$, i.e., the probability of the parameters, $\theta$, given the data, $y$. At the foundation of the theory lies Bayes' theorem:

$$p(\theta|y) = \frac{\mathcal{L}(y|\theta)\pi(\theta)}{\int \mathcal{L}(y|\theta)\pi(\theta)d\theta}. \quad (11)$$

The numerator on the right side of Equation (11) represents the product of the model likelihood, $\mathcal{L}(y|\theta)$, i.e., the probability that the data, $y$, were obtained given the model parameters, $\theta$, and the prior distribution, $\pi(\theta)$, which represents our state of knowledge before considering the new data. The normalization factor appearing in the denominator, called the evidence, describes the probability of obtaining the data considering all possible parameter values.

In the Bayesian framework, the concept of hierarchical Bayesian models is of particular interest when accounting for different effects and processes that impact the measured data (Parent & Rivot 2012; de Souza et al. 2015, 2016; Hilbe et al. 2017). The underlying idea is to decompose higher-dimensional problems into a number of probabilistically linked lower-dimensional substructures. Hierarchical Bayesian models allow for a consistent inclusion of different types of uncertainties into the model, thereby solving inferential problems that are not amenable to traditional statistics (e.g. Trotta 2017).

### 3.2. *A toy example*

Figure 4 depicts a toy nuclear counting experiment to illustrate an inherently hierarchical statistical structure. The vertical axis shows the number of counts, and the different layers of variabilities are indicated on the horizontal axis. The theoretical mean value of the true number of nuclear decays, $y$ (grey dot), is unknown. In statistical parlance, $y$ is called a latent or hidden variable, representing the boundary between the theoretical and observable world. The actual number of decays, $y'$ (brown dot), differs from the theoretical mean value because of the stochastic nature of a nuclear decay or reaction process. We can write

$$y' = y + \epsilon_{stoc}, \quad (12)$$

where $\epsilon_{stoc}$ quantifies the stochastic contribution that perturbs $y$.

The quantity $y'$ is also unobservable since we have not considered experimental effects yet. Typically, data are subject to systematic and statistical effects. The systematic contribution, $\epsilon_{syst}$, which affects all data points of a given experiment equally, perturbs the number of

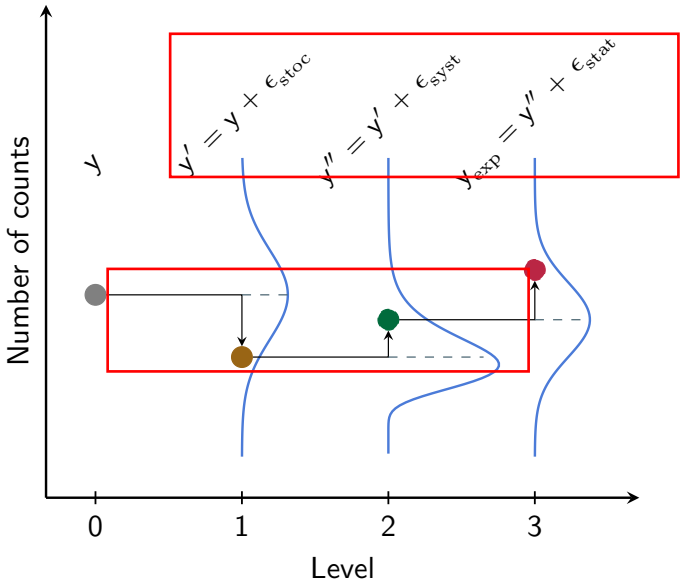


**Figure 4.** Example of a counting experiment. The true (but unknown) value of the quantity, $y$ (here the mean number of counts; gray circle) is perturbed at each level by different effects: (i) intrinsic stochasticity ($\epsilon_{stoc}$; brown circle), (ii) experimental systematic effects ($\epsilon_{syst}$; green circle), (iii) experimental statistical effects ($\epsilon_{stat}$; red circle). The Bayesian model is constructed to estimate the posterior density for the true value of $y$ (gray circle) from the actual measurement (red circle). The probability densities at each level are shown as solid blue lines.

counts (brown dot) and gives rise to the green dot. We can write

$$y'' = y' + \epsilon_{syst}, \quad (13)$$

Finally, the statistical contribution, $\epsilon_{stat}$, which differs for each data point of a given experiment, also perturbs the number of counts (green dot) and gives rise to the measured value (red dot), according to

$$y_{exp} = y'' + \epsilon_{stat}. \quad (14)$$

It is straightforward to construct the hierarchical Bayesian model that incorporates all of these different layers of variability, as explained in the next section. The goal is to estimate the posterior density for the unobservable theoretical mean, $y$, based on the measured value of $y_{exp}$.

### 3.3. *Likelihoods and priors*

We will next discuss how to construct likelihoods to quantify the different layers of uncertainty affecting the $^3$He(d,p)$^4$He and d($^3$He,p)$^4$He data. Throughout this work, we evaluate the Bayesian models using JAGS ("Just Another Gibbs Sampler"), a domain-specific language for analysis of Bayesian hierarchical models using

Markov chain Monte Carlo (Plummer 2003). Specifically, we used the RJAGS package to interface JAGS with the R language (Team 2010).

Running a Bayesian model in JAGS refers to generating random samples from the posterior distribution of model parameters. This requires the definition of the model, likelihoods, and priors, as well as the initialization, adaptation, and monitoring of the Markov chain. We implemented a new JAGS module to allow for sampling of a theoretical S-factor model for the $^3$He(d,p)$^4$He reaction based on the R-matrix formalism (Section 2), including the effect of electron screening.

#### 3.3.1. *Stochastic effects*

We will first discuss the treatment of a stochastic process. Suppose an experimental S-factor, $S_{exp}$, is free of systematic and statistical measurement uncertainties ($\epsilon_{syst} = 0$, and $\epsilon_{stat} = 0$), but is subject to an unknown stochastic effect ($\epsilon_{stoc} \neq 0$). If the variable under study is continuous, one can assume in the simplest case a Gaussian noise, with standard deviation of $\sigma_{stoc}$. The model likelihood connecting experiment with theory, assuming a vector of model parameters, $\theta$, is then given by:

$$\mathcal{L}(S_{exp}|\theta) = \prod_{i=1}^{N} \frac{1}{\sqrt{2\pi\sigma_{stoc}^2}} \exp\left[-\frac{(S_{exp;i} - S_i(\theta))^2}{2\sigma_{stoc}^2}\right], \tag{15}$$

where $S_i(\theta)$ is the model S-factor (obtained from R-matrix theory), while the product runs over all data points, $N$, labeled by $i$. In symbolic notation, this expression can be written as:

$$S_{exp;i} \sim \text{Normal}(S_i(\theta), \sigma_{stoc}^2), \tag{16}$$

implying that the experimental S-factor datum, $i$, is sampled from a normal distribution, with a mean equal to the true value, $S_i(\theta)$, and a variance of $\sigma_{stoc}^2$.

#### 3.3.2. *Statistical effects*

Any experiment is subject to measurement uncertainties, which are the consequence of an inherent imperfection of the data-taking process. Suppose the measurement uncertainties are solely given by statistical effects and that the likelihood can be described, in the simplest case, by a normal probability density. The likelihood for such model can be written symbolically as:

$$S_{exp;i} \sim \text{Normal}(S_i(\theta), \sigma_{stat;i}^2). \tag{17}$$

where $\sigma_{stat;i}^2$ represents the variance of the normal density for datum $i$. Unlike the uncertainty caused by the effect of stochasticity (Section 3.3.1), statistical uncertainties can be reduced by improving the data collection procedure and by collecting more data.

When both statistical and stochastic uncertainties are present, the model can be easily extended to accommodate both effects. The likelihood for such model is given by the nested expressions:

$$S_i' \sim \text{Normal}(S_i(\theta), \sigma_{stoc}^2), \tag{18}$$

$$S_{exp;i} \sim \text{Normal}(S_i', \sigma_{stat;i}^2). \tag{19}$$

These expressions provide an intuitive view of how a chain of probabilistic disturbances can be combined into a hierarchical structure. First, stochastic effects, quantified by the standard deviation $\sigma_{stoc}$ of a normal probability density, perturb the theoretical value of a given S-factor datum, $S_i(\theta)$, to produce a value of $S_i'$; second, the latter value is in turn perturbed by the statistical uncertainty, quantified by the standard deviation $\sigma_{stat;i}$ of a normal probability density, to produce the measured value $S_{exp;i}$. The above demonstrates how an effect impacting the data can be implemented in a straightforward manner into a Bayesian data analysis.

#### 3.3.3. *Systematic effects*

Systematic uncertainties are usually not reduced by combining the results from different measurements or by collecting more data. Reported systematic uncertainties are based on assumptions made by the experimenter, are model-dependent, and follow vaguely known probability distributions (Heinrich & Lyons 2007). In a nuclear counting experiment, systematic effects impact the overall normalization by shifting all points of a given data set into the same direction, and they are often quantified by a multiplicative factor.

For example, if the systematic uncertainty for a given data set is reported as $\pm 10\%$, the factor uncertainty, f..u., amounts to 1.10. A useful distribution for normalization factors is the lognormal probability density:

$$f(x) = \frac{1}{\sigma_L x\sqrt{2\pi}} \exp\left[-\frac{(\ln x - \mu_L)^2}{2\sigma_L^2}\right], \tag{20}$$

which is characterized by two quantities, the location parameter, $\mu_L$, and the shape parameter, $\sigma_L$. The median value of the lognormal distribution is given by $e^{\mu_L}$, while the factor uncertainty, for a coverage probability of 68%, is $e^{\sigma_L}$. In our model, we include a systematic effect as an informative lognormal prior with a median of 1.0, i.e., $\mu_L = 0$, and the f..u. given by the systematic uncertainty.

In our model, we can include systematic uncertainties using the nested expressions:

$$S_i' \sim \text{Normal}(S_i(\theta), \sigma_{stoc}^2), \tag{21}$$

$$S_{exp;i,j} \sim \text{Normal}(\xi_j S_i', \sigma_{stat;i}^2), \tag{22}$$

where $\xi_j$ denotes the normalization factor for data set $j$, which is drawn from a lognormal distribution.

#### 3.3.4. *Priors*

To test the effects of different priors on our results, we consider two scenarios in the data fitting, which are summarized in Table 1. In the first scenario ("case I"), we employ moderately informative priors for $E_0$ and fixed values for the channel radii ($a_d = 6$ fm, $a_p = 5$ fm), consistent with Barker (2007). Previous estimates of the deuteron reduced width are near 1.0 MeV (Coc et al. 2012), which corresponds to values ~~very~~ close to the Wigner limit (Wigner & Eisenbud 1947). To allow some flexibility around this estimate, we use a broad prior for the reduced widths, i.e., half-normal distributions centered at zero, with a standard deviation of 3.0 MeV. We will also set the eigenvalue, $E_0$, equal to the energy, $E_r$, at which the level shift is zero according to Equations (5) and (9).

In the second scenario ("case II"), we adopt overall weaker priors. Lane & Thomas (1958), recommend to chose the boundary condition, $B_c$, in the one-level approximation so that the eigenvalue $E_0$ lies within the width of the observed resonance. Thus we chose for $E_0$ a uniform prior between 0.1 MeV and 0.4 MeV, i.e., U(0.1, 0.4). For $E_r$, i.e., the energy at which the level shift is zero according to Equations (5) and (9), we chose a broad half-normal prior, centered at zero, with a standard deviation of 1.0 MeV. Woods et al. (1988) reported a best channel radius of $5.5 \pm 1.0$ fm for the $^5$He and $^5$Li systems. We then adopt for the channel radii uniform priors, in the range 2-10 fm. For the reduced widths, the priors are the same as for Case I.

As for the electron screening potential, Aliotta et al. (2001) obtained values of $U_e = 146 \pm 5$ eV for the d($^3$He,p)$^4$He reaction, and $U_e = 201 \pm 10$ eV for the $^3$He(d,p)$^4$He reaction. Since $U_e$ is a positive quantity, we will adopt a weakly informative prior given by a half-normal distribution, centered at zero, with a standard deviation of 100 keV for both scenarios.

As already pointed out above, lognormal priors are adopted for the normalization factors, $\xi_j$, of each experiment, $j$. They are given by:

$$\xi_j \sim \text{LogNormal}(0, \ln(1 + \sigma^2_{syst;j})), \tag{23}$$

where $\sigma_{syst;j}$ denotes the systematic uncertainty for experiment $j$.

## 4. ANALYSIS OF $^3$He(d,p)$^4$He AND DATA

The current status of the available data for the $^3$He(d,p)$^4$He and d($^3$He,p)$^4$He reactions is discussed in detail in Appendix A. For the present analysis, we adopt the results of Zhichang et al. (1977); Krauss et al. (1987); Möller & Besenbacher (1980); Geist et al. (1999); Costantini et al. (2000); Aliotta et al. (2001), because only these data sets allow for a separate estimation of statistical and systematic uncertainties. In total, our compilation includes 214 data points at center-of-mass energies between 4.2 keV and 471 keV.

**Table 1.** Prior choices for Case I (moderately informative) and II (weakly informative)[a].

| | Case I | Case II |
|---|---|---|
| $E_0$ | HalfNormal(0,$1^2$) | Uniform(0.1, 0.4) |
| $E_r$ | $E_0$ | HalfNormal(0, $1^2$) |
| $\gamma_d^2$ | HalfNormal(0,$3^2$) | HalfNormal(0,$3^2$) |
| $\gamma_p^2$ | HalfNormal(0,$3^2$) | HalfNormal(0,$3^2$) |
| $a_d$ | 6 | U(2,10) |
| $a_p$ | 5 | U(2,10) |
| $U_e$ | HalfNormal(0, $0.1^2$) | HalfNormal(0, $0.1^2$) |
| $\xi$ | LogNormal(0, $\sigma_L^2$)[b] | LogNormal(0, $\sigma_L^2$)[b] |

[a] Units for energies are in MeV, while those for the channel radii are in fm.
[b] $\sigma_L^2 \equiv \ln(1 + \sigma^2_{syst})$.

### 4.1. *Results for Case I priors*

We will first discuss the results of a Bayesian analysis using just three R-matrix parameters ($E_0$, $\gamma_d^2$, and $\gamma_p^2$). The channel radii and boundary condition parameters are kept fixed at $a_d = 6.0$ fm, and $a_p = 5.0$ fm. Our model then contains a total of 13 parameters ~~of interest~~: three R-matrix parameters, seven normalization factors ($\xi_1, \ldots, \xi_7$), the stochastic uncertainty ($\sigma_{stoc}$), and the two screening potentials ($U_{e1}$,$U_{e2}$) for the $^3$He(d,p)$^4$He and d($^3$He,p)$^4$He reactions respectively. The full hierarchical Bayesian model can be summarized as:

$$\begin{aligned}
&\text{Likelihood} \\
&\quad S_i' \sim \text{Normal}(S_i(\theta) e^{\pi\eta(U_{ek}/E_{exp;i})}, \sigma^2_{stoc}) \\
&\quad S_{exp;i,j} \sim \text{Normal}(\xi_j S_i', \sigma^2_{stat;i}) \\
&\text{R-matrix Parameters} \\
&\quad \theta \equiv (E_0, \gamma_d^2, \gamma_p^2) \\
&\text{Priors} \\
&\quad \xi_j \sim \text{LogNormal}(0, \ln(1 + \sigma^2_{\text{syst;j}})) \\
&\quad E_0 \sim \text{HalfNormal}(0, 1^2) \\
&\quad (\gamma_d^2, \gamma_p^2) \sim \text{HalfNormal}(0, 3^2) \\
&\quad U_{ek} \sim \text{HalfNormal}(0, 0.1^2)
\end{aligned} \tag{24}$$

The first layer accounts for the effects of an inherent stochastic uncertainty and electron screening, while the second layer describes the effects of systematic and statistical uncertainties. The indices denote the number of data sets ($j = 1, ..., 7$), data points ($i = 1, ..., 214$), and the two possibilities for electron screening ($k = 1$ or 2) depending on the kinematics of the experiment.

The above model was implemented as an extra module in JAGS, and we ran MCMC sampling to get posteriors for all 13 parameters of interest. We generated random samples using five independent Markov chains, each of length 25,000. This ensures that the Monte Carlo fluctuations are negligible compared to the statistical and systematic uncertainties. The lengths of the initial adapting and burn-in phases were set to 10,000 steps. The fitted S-factor is displayed at Figure 5. The solid lines show three solutions and their respective credible intervals: the bare-nucleus S-factor (purple), i.e. the estimated S-factor free from the effects of electron screening, and the S-factors for d($^3$He,p)$^4$He (red) and $^3$He(d,p)$^4$He (gray). The inset magnifies the region where the effects of electron screening become important.

Figure 6 presents the one- and two-dimensional marginalized posterior densities of the R-matrix parameters $E_0$, $\gamma_d^2$, $\gamma_p^2$, and the electron screening potential $U_e$. In addition, we included the posteriors for the derived S-factor at zero energy for comparison with previous studies. The contours in the diagonal panels depict 50%, 95%, and 99.7% credible intervals around the marginal posterior mean.

Summary statistics for the model parameters are presented at Table 2 alongside with previous estimates. The estimated values for the reduced widths are substantially smaller than the previous estimate from Barker (2007).

Table 2 also summarizes our estimates $U_{e1}$ = 193 ± 10 eV ($^3$He(d,p)$^4$He), and $U_{e2}$ = 105 ± 10 eV (d($^3$He,p)$^4$He). The values for $^3$He(d,p)$^4$He are consistent with previous estimates from Barker (2007), and Descouvemont et al. (2004) within the uncertainties, but slightly smaller than Aliotta et al. (2001). The estimated screening potential for d($^3$He,p)$^4$He shows a good agreement with Aliotta et al. (2001), but it is smaller than the one obtained by Descouvemont et al. (2004). We shall note that the current and previous estimated values are still larger than the so-called adiabatic limit – the difference in electron binding energies between the colliding atoms and the compound atom – $U_e$ = 65 eV for d($^3$He,p)$^4$He, and $U_e$ = 120 eV for $^3$He(d,p)$^4$He (e.g., Aliotta et al. 2001), and such discrepancy are yet to be explained. Table 2 also displays our estimate for the intrinsic scatter, $\sigma_{stoc}$, and the S-factor at zero energy, which despite the differences in datasets and methodologies is in reasonable agreement with previous estimates.

**Table 2.** Results for the 13-parameter Bayesian fit.

| Parameter | Present | Previous |
|---|---|---|
| $E_0$ (MeV) | $0.346^{+0.004}_{-0.004}$ | 0.200[a] |
| $E_r$ (MeV) | $0.346^{+0.004}_{-0.004}$ | 0.427[a] |
| $\gamma_p^2$ (MeV) | $0.0237^{+0.0008}_{-0.0007}$ | 0.0506[a] |
| $\gamma_d^2$ (MeV) | $0.985^{+0.042}_{-0.037}$ | 1.9432[a] |
| $S_0$ (MeV b) | $6.135^{+0.118}_{-0.108}$ | $5.9^{+0.3}_{-0.3}$[b], 6.7[c], 6.05[d] |
| $\sigma_{stoc}$ (MeV) | $0.54^{+0.031}_{-0.031}$ | ✗ |
| $U_{e1}$ (eV) | $194.14^{+9.94}_{-9.80}$ | 194[a], $201^{+10}_{-10}$[b], $219^{+7}_{-7}$[c] |
| $U_{e2}$ (eV) | $104.85^{+9.73}_{-10.30}$ | $146^{+5}_{-5}$[b], $109^{+9}_{-9}$[c] |
| $\zeta_1$ (Ali01a) | $0.992^{+0.017}_{-0.017}$ | ✗ |
| $\zeta_2$ (Ali01b) | $1.019^{+0.019}_{-0.019}$ | ✗ |
| $\zeta_3$ (Cos00) | $1.045^{+0.024}_{-0.024}$ | ✗ |
| $\zeta_4$ (Gei99) | $0.968^{+0.018}_{-0.018}$ | ✗ |
| $\zeta_5$ (Kra87) | $1.003^{+0.021}_{-0.021}$ | ✗ |
| $\zeta_6$ (Mol80) | $1.012^{+0.019}_{-0.019}$ | ✗ |
| $\zeta_7$ (Zhi77) | $0.971^{+0.018}_{-0.018}$ | ✗ |

[a] One-level R-matrix fit from Barker (2007), Table II, row C, using Geist et al. (1999) data.

[b] From Descouvemont et al. (2004).

[c] From Aliotta et al. (2001); no uncertainty estimates were provided.

[d] Two-level R-matrix fits from Barker (2007), Table I, row C, using La Cognata et al. (2005) and Aliotta et al. (2001) data.

The probability distributions for the normalization factors are displayed in Figure 7 and their summary statistics are subsumed in the bottom part of Table 2. The vertical dashed red line represents zero systematic effects (i.e., a normalization factor of unity). The normalization factors are mostly below 5% with 95% probability, indicating that reliable systematic uncertainty estimates were adopted for the data sets used in the present analysis.

### 4.2. *Results for Case II priors*

The results discussed heretofore were obtained assuming fixed values for the channel radii and boundary condition parameters. This section explores the impact of varying these quantities in the fit procedure. The

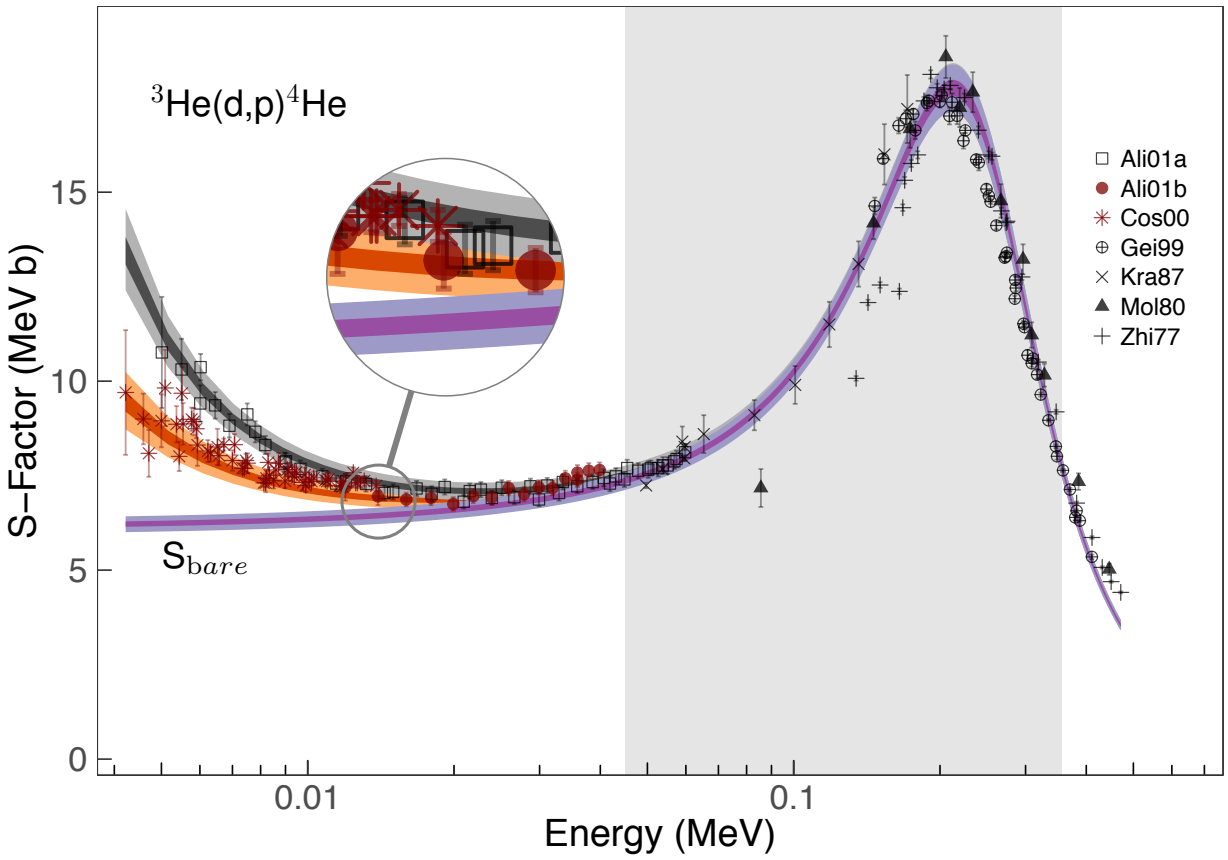


**Figure 5.** Astrophysical S-factor $^3$He(d,p)$^4$He for bare and screened nuclei versus center-of-mass. The symbols show the different experiments taken into account in the present analysis: open square (□; Aliotta et al. 2001); red solid circle (•; Aliotta et al. 2001); red asterisk (∗; Costantini et al. 2000); circled cross (⊕; Geist et al. 1999); times sign (×; Krauss et al. 1987); solid triangle (▲; Möller & Besenbacher 1980); cross (+; Zhichang et al. 1977), but see also appendix A for a more detailed description. The uncertainty bars refer to (1-$\sigma$) statistical uncertainties only. The solid lines show the results of the present Bayesian analysis: (purple) bare-nucleus S-factor; (red) S-factor for d($^3$He,p)$^4$He reaction; (gray) S-factor for $^3$He(d,p)$^4$He reaction. The shaded areas depicts 50%, and 95% credible intervals around the mean. The inset shows a magnified view of the region where the three curves diverge.

Bayesian model from Equation (24) can be straightforwardly extended including priors on $E_r$, $a_d$, and $a_p$ (Table 1, Case II).

Table 3 lists the R-matrix parameters estimates for our extended model. The normalization factors, stochastic uncertainty and screening potentials are ~~virtually~~ unaffected by varying the channel radii or boundary condition parameters and are not shown. Te estimated values for $E_0$, $E_r$ are in good agreement with Barker (2007), unlike the reduced widths, $\gamma_p^2$ and $\gamma_d^2$, whose discrepancy is heavily affected by the difference in the channel radii. We shall note that the eigenenergy, $E_0$, has a large uncertainty, mostly covering the entire range of its prior. This is caused by the degeneracy with $E_r$, since variations in $E_0$ over the width of the observed resonance can be compensated by adjusting the value of $E_r$, providing equally good results.

Our mean estimates for the channel radii are smaller than previously fixed adopted values (Barker 2007), but in marginal agreement within the uncertainties.

~~Next section discuss the effects of our prior choices in the estimated reaction rates and how it compares with previous estimates.~~

## 5. BAYESIAN REACTION RATES

The non-resonant thermonuclear reactions rates per particle pair is given by the Maxwellian-averaged rate,

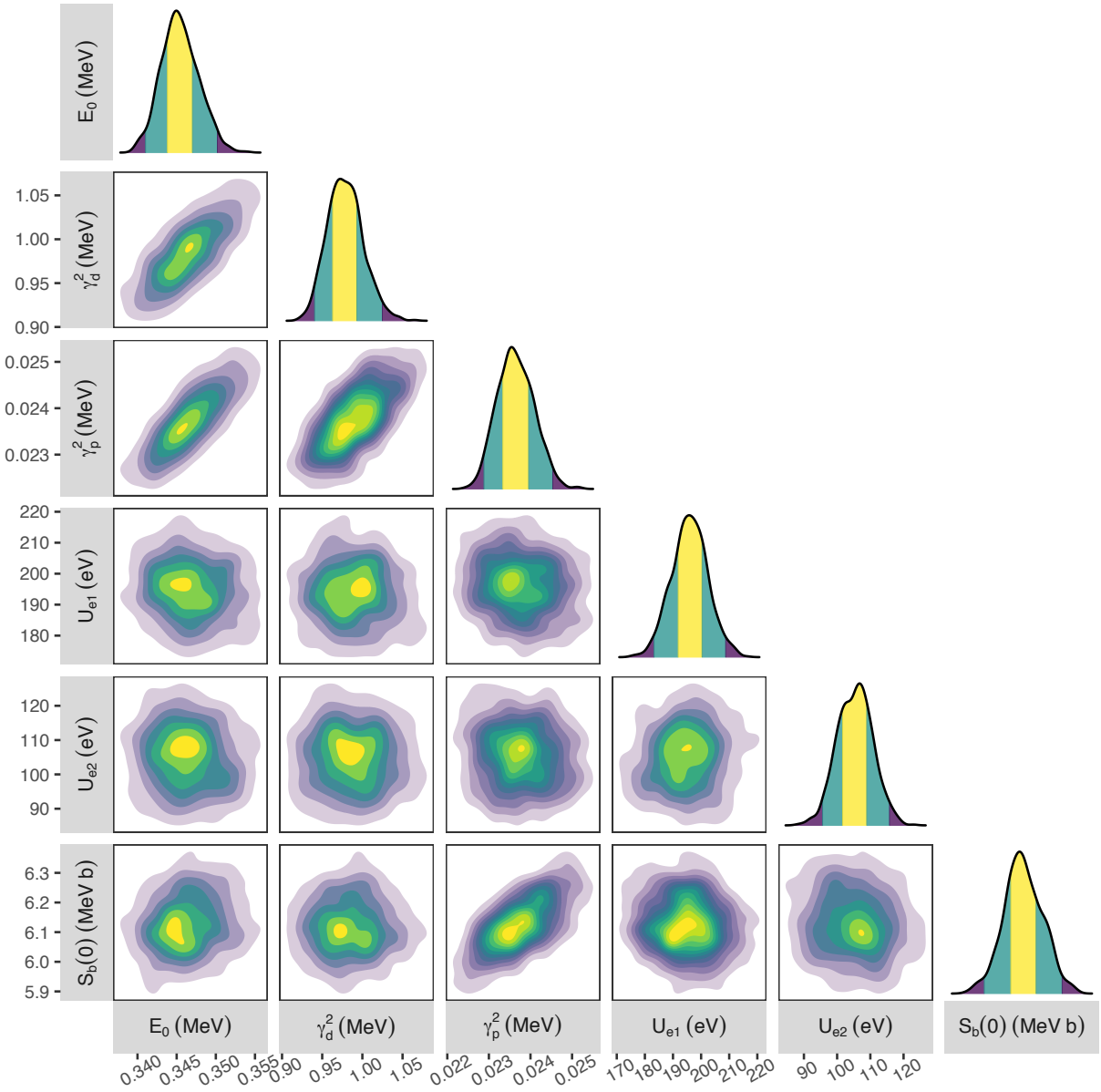


**Figure 6.** One- and two-dimensional marginalized posterior densities for the R-matrix parameters ($E_0$, $\gamma_d$, $\gamma_p$, $U_e$, and $S_b(0)$); see Section 2. The results were obtained for "case I" (see Section 3.3.4).

$\langle\sigma\nu\rangle$, times ~~the~~ Avogrado's number $N_A$:

$$N_A \langle\sigma\nu\rangle = N_A \frac{(8/\pi)^{1/2}}{\mu_0^{1/2}(k_B T)^{3/2}} \int_0^\infty E\sigma(E) e^{-E/k_B T} dE, \quad (25)$$

where $\sigma(E) \equiv S(E)e^{-2\pi\eta}/E$ is the reaction cross section at the center-of-mass incident energy $E$ ~~$= \mu v^2/2$ with $v$ being the relative velocity~~. The term $\mu_0 = m_a m_b/(m_a + m_b)$ is the reduced mass with $m_A$ and $m_a$ standing for the masses of target (a) and projectile (b) ~~nuclei~~, $k_B$ is the Boltzmann constant, $T$ the temperature, $\sigma$ the cross section.

We estimate the reaction rates on a grid of temperatures from 1 MK to 10 GK. The ~~presented~~ temperature grid is chosen to be consistent with previous works ~~(Descouvemont et al. 2004),~~ and to allow a seamless incorporation into the STARLIB library (Sallaska et al. 2013).

To stress the robustness of our results against different priors choices, we provide a comparison between the predicted rates from Case I and Case II. ~~To guide the eyes, all values are normalized to the median rates of Case II.~~ The left panel of Figure 8 displays the results. The 1-$\sigma$ credible interval for Case II, which we will refer

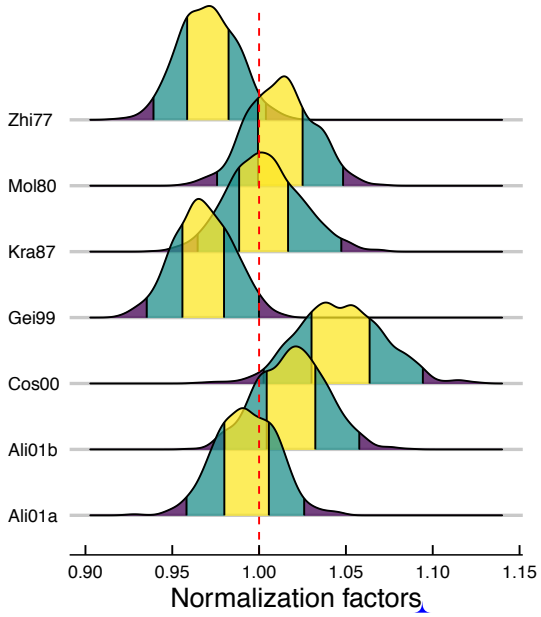


**Figure 7.** Posterior of the normalization factors, $\xi_i$, for each of the seven datasets. The colored areas depicts 50% 95% and 99.5% credible intervals, respectively. For the data set labels, see Figure 5.

**Table 3.** Results for the 15-parameter Bayesian fit. Only those parameters that have changed from Case I to Case II are shown.

| Parameter | Present | Previous |
|---|---|---|
| $E_0$ (MeV) | $0.268^{+0.180}_{-0.123}$ | 0.200[a] |
| $E_r$ (MeV) | $0.442^{+0.067}_{-0.084}$ | 0.427[a] |
| $\gamma_p^2$ (MeV) | $0.171^{+0.293}_{-0.100}$ | 0.0506[a] |
| $\gamma_d^2$ (MeV) | $4.352^{+1.314}_{-1.663}$ | 1.9432[a] |
| $a_p$ (fm) | $2.518^{+2.718}_{-0.455}$ | 5[a] |
| $a_d$ (fm) | $4.495^{+0.362}_{-0.164}$ | 6[a] |

[a] One-level R-matrix fit from Barker (2007), Table II, row C, using Geist et al. (1999) data.

as our recommended rates, are shown as a gray band, and the orange band represents the ratio between both rates. Note the consistency within less than 3% for the entire range of Astrophysical interest.

The right panel of Figure 8 compares our present recommended rates with previous estimate from Descouvemont et al. (2004), whose 1-$\sigma$ confidence interval is shown as purple bands. In comparison to our present rates, the rates from Descouvemont et al. are lower by up to 4-5% at lower temperatures and higher by up to 2.5% at temperatures of interest for the BBN.

Numerical reaction rate values are listed in Table 8. The recommended rates are computed as the 50th percentile of the probability density, while the rate factor uncertainty is given by f.u. $= e^{\sigma_L}$, with $\sigma_L$ being the standard deviation of the posterior.

## 6. SUMMARY AND CONCLUSIONS

The Big-Bang nucleosynthesis represents a milestone in the Universe evolution, marking the production of the first light nuclides. Accurate measurements of the nuclear reaction rates occurring on this epoch are paramount to estimate the primordial abundance of the first elements. However, the connection between the theoretical cross-section, subsumed by the Astrophysical S-factor, and the S-factors obtained by nuclear physics experiments is subtle. The data is subject to several layers of uncertainty, including: intrinsic scatter, systematic effects, error-in-measurements and the effects of the electron screening potential. Such stratified error-structure cannot be fully accountable by ready-to-use procedures such as $\chi^2$ minimization.

To overcame such limitation, we presented the first hierarchical Bayesian R-matrix analysis of the $^3$He(d,p)$^4$He S-factors and thermonuclear reaction rates. Our approach consistently incorporates for all known sources of uncertainties, providing a testbed for future studies, in which a statistically sound analysis is required.

We would like to thank xxx for their input and feedback. This work was supported in part by NASA under the Astrophysics Theory Program grant 14-ATP14-0007 and the U.S. DOE under Contract No. DE-FG02-97ER41041 (UNC) and DE-FG02-97ER41033 (TUNL).

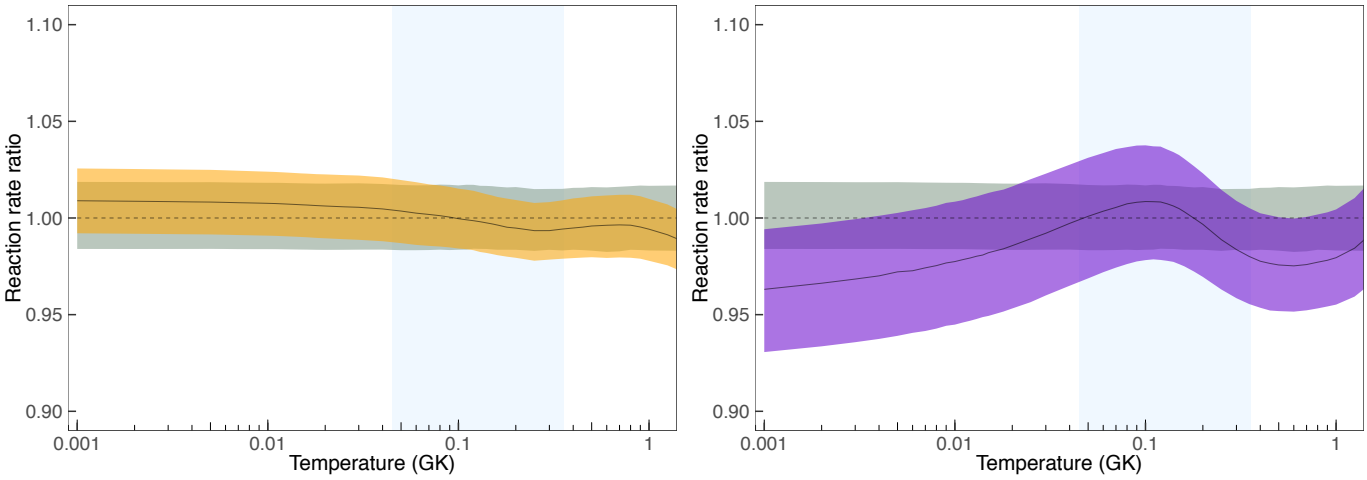


(a) (b)

**Figure 8.** a) The gray band corresponds to our new ~~recommended rate~~, while the orange band depicts Case I. The bands depicts a 68% coverage probability. All rates are normalized to Case II. b) The gray band corresponds to our new Bayesian rate, while the purple band depicts the ratio between Descouvemont et al. (2004) rates and the present recommended rates.

.

**Table 4.** Recommended $^3$He(d,p)$^4$He reaction rates.[a]

| T (GK) | Rate | f.u. | T (GK) | Rate | f.u. |
|---|---|---|---|---|---|
| 0.001 | 3.6972E-19 | 1.018 | 0.14 | 2.9390E+05 | 1.017 |
| 0.002 | 6.3684E-13 | 1.018 | 0.15 | 3.9326E+05 | 1.017 |
| 0.003 | 6.5806E-10 | 1.018 | 0.16 | 5.1391E+05 | 1.017 |
| 0.004 | 5.1790E-08 | 1.018 | 0.18 | 8.2668E+05 | 1.016 |
| 0.005 | 1.1476E-06 | 1.018 | 0.2 | 1.2483E+06 | 1.016 |
| 0.006 | 1.2137E-05 | 1.018 | 0.25 | 2.8651E+06 | 1.016 |
| 0.007 | 7.9562E-05 | 1.018 | 0.3 | 5.3982E+06 | 1.016 |
| 0.008 | 3.7437E-04 | 1.018 | 0.35 | 8.8923E+06 | 1.016 |
| 0.009 | 1.3836E-03 | 1.018 | 0.4 | 1.3291E+07 | 1.017 |
| 0.01 | 4.2592E-03 | 1.018 | 0.45 | 1.8470E+07 | 1.017 |
| 0.011 | 1.1370E-02 | 1.018 | 0.5 | 2.4283E+07 | 1.017 |
| 0.012 | 2.7090E-02 | 1.018 | 0.6 | 3.7138E+07 | 1.017 |
| 0.013 | 5.8830E-02 | 1.018 | 0.7 | 5.0648E+07 | 1.017 |
| 0.014 | 1.1832E-01 | 1.018 | 0.8 | 6.3958E+07 | 1.017 |
| 0.015 | 2.2310E-01 | 1.018 | 0.9 | 7.6539E+07 | 1.017 |
| 0.016 | 3.9826E-01 | 1.018 | 1 | 8.8077E+07 | 1.017 |
| 0.018 | 1.1091E+00 | 1.018 | 1.25 | 1.1178E+08 | 1.018 |
| 0.02 | 2.6761E+00 | 1.018 | 1.5 | 1.2857E+08 | 1.018 |
| 0.025 | 1.5564E+01 | 1.018 | 1.75 | 1.3983E+08 | 1.018 |
| 0.03 | 5.9371E+01 | 1.018 | 2 | 1.4694E+08 | 1.018 |
| 0.04 | 4.1527E+02 | 1.017 | 2.5 | 1.5305E+08 | 1.018 |
| 0.05 | 1.6497E+03 | 1.017 | 3 | 1.5285E+08 | 1.019 |
| 0.06 | 4.7173E+03 | 1.017 | 3.5 | 1.4951E+08 | 1.019 |
| 0.07 | 1.0913E+04 | 1.017 | 4 | 1.4467E+08 | 1.019 |
| 0.08 | 2.1809E+04 | 1.017 | 5 | 1.3355E+08 | 1.02 |
| 0.09 | 3.9189E+04 | 1.017 | 6 | 1.2260E+08 | 1.021 |
| 0.1 | 6.4977E+04 | 1.017 | 7 | 1.1274E+08 | 1.021 |
| 0.11 | 1.0123E+05 | 1.017 | 8 | 1.0408E+08 | 1.022 |
| 0.12 | 1.5003E+05 | 1.017 | 9 | 9.6489E+07 | 1.023 |
| 0.13 | 2.1355E+05 | 1.017 | 10 | 8.9812E+07 | 1.024 |

[a] In units of $cm^3$ ~~$mol^1\ s^1$~~, corresponding to the 50th percentiles of the rate probability density function. The rate factor uncertainty, f.u., corresponds to a coverage probability of 68% and is obtained from the 16th and 84th percentiles.

# APPENDIX

## A. NUCLEAR DATA FOR THE $^3$HE(D,P)$^4$HE REACTION

### A.1. *The $^3$He(d,p)$^4$He data of Zhichang et al. (1977)*

The cross section data of Zhichang et al. (1977), as reported in EXFOR (2017), originate from a private communication by the authors and were adopted from Figure 2 of the original article. The derived experimental S-factors, together with their statistical uncertainties ($\approx 0.6\%$) are listed in Table 5. The estimated systematic uncertainty is 3.4%, including the effects of target, solid angle, and beam intensity.

**Table 5.** The $^3$He(d,p)$^4$He data of Zhichang et al. (1977).

| $E_{c.m.} \pm \Delta E_{c.m.}$ (MeV) | $S \pm \Delta S_{\rm stat}$[a] (MeVb) | $E_{c.m.} \pm \Delta E_{c.m.}$ (MeV) | $S \pm \Delta S_{\rm stat}$[a] (MeV b) |
|---|---|---|---|
| 0.1344±0.0048 | 10.074±0.060 | 0.2559±0.0042 | 15.950±0.095 |
| 0.1422±0.0047 | 12.080±0.072 | 0.2676±0.0042 | 14.505±0.087 |
| 0.1506±0.0047 | 12.544±0.075 | 0.2736±0.0041 | 14.194±0.085 |
| 0.1650±0.0046 | 12.375±0.074 | 0.2748±0.0041 | 14.231±0.085 |
| 0.1677±0.0045 | 14.590±0.087 | 0.2949±0.0041 | 12.757±0.076 |
| 0.1692±0.0045 | 15.314±0.092 | 0.3186±0.0041 | 10.505±0.063 |
| 0.1746±0.0045 | 15.760±0.095 | 0.3468±0.0040 | 9.188±0.055 |
| 0.1800±0.0044 | 15.987±0.096 | 0.3822±0.0040 | 6.773±0.040 |
| 0.1854±0.0044 | 17.415±0.104 | 0.4110±0.0039 | 5.863±0.035 |
| 0.1914±0.0044 | 18.116±0.109 | 0.4314±0.0038 | 5.071±0.030 |
| 0.1974±0.0044 | 17.763±0.107 | 0.4500±0.0037 | 4.695±0.028 |
| 0.2040±0.0044 | 17.728±0.106 | 0.4710±0.0037 | 4.411±0.026 |
| 0.2100±0.0044 | 17.825±0.107 | 0.5070±0.0036 | 3.761±0.022 |
| 0.2247±0.0043 | 17.502±0.105 | 0.5466±0.0035 | 3.002±0.018 |
| 0.2400±0.0043 | 16.640±0.099 | 0.5772±0.0034 | 2.999±0.018 |
| 0.2520±0.0042 | 15.987±0.096 | 0.6135±0.0033 | 2.364±0.014 |

[a] Systematic uncertainty: 3.4%.

### A.2. *The $^3$He(d,p)$^4$He and d($^3$He,p)$^4$He data of Krauss et al. (1987)*

The Krauss et al. (1987) experiments took place at the ion accelerators in Münster and Bochum. Table 3 in Krauss et al. (1987) lists measured S-factors and statistical uncertainties. A normalization uncertainty of 6% originates from an absolute $^3$He(d,p)$^4$He cross section measurement at a center-of-mass energy of 59.66 keV, to which a 5% uncertainty caused by variations in the alignment of beam and gas jet target profiles has to be added for the Münster data. Hence, we adopt a systematic uncertainty of 6.0% for the Bochum data and, following the authors, a value of 7.8% for the Münster data. Note that Krauss et al. (1987) do not report separately the results for $^3$He(d,p)$^4$He and d($^3$He,p)$^4$He. Since this distinction is important below a center-of-mass energy of 50 keV, we disregard all of their data points in this energy range. The data adopted for our analysis are listed in Table 6.

### A.3. *The d($^3$He,p)$^4$He data of Möller & Besenbacher (1980)*

In this experiment, the d($^3$He,p)$^4$He differential cross section was measured at two angles, relative to the d(d,p)$^3$H cross section. The total cross section was calculated using the angular distributions from Yarnell et al. (1953). The statistical error is less than 3%, except at the lowest energy (7%). The systematic error, which arises from the

**Table 6.** The $^3$He(d,p)$^4$He and d($^3$He,p)$^4$He data of Krauss et al. (1987)[a].

| $E_{c.m.}$ (MeV) | $S \pm \Delta S_{\rm stat}$[b] (MeVb) | $E_{c.m.}$[d] (MeV) | $S \pm \Delta S_{\rm stat}$[b] (MeVb) |
|---|---|---|---|
| 0.04970[c] | 7.24±0.07 | 0.0830 | 9.1±0.4 |
| 0.05369[c] | 7.67±0.08 | 0.1007 | 9.9±0.5 |
| 0.05900[d] | 8.4±0.4 | 0.1184 | 11.5±0.6 |
| 0.05952[c] | 7.96±0.08 | 0.1360 | 13.1±0.6 |
| 0.05966[c] | 8.26±0.08 | 0.1537 | 16.0±0.8 |
| 0.0653[d] | 8.6±0.5 | 0.1713 | 17.2±0.9 |

[a] We disregarded all data points below a center-of-mass energy of 50 keV (see text).

[b] For some data points without reported statistical uncertainty, we assumed a value of 1%.

[c] Bochum data; S-factor systematic uncertainty: 6.0%.

[d] Münster data; S-factor systematic uncertainty: 7.8%.

normalization, the d(d,p)$^3$H cross section, and the anisotropy coefficient, amounts to 3.9%. The EXFOR cross section data were presumably scanned from Fig. 3 of (Möller & Besenbacher 1980). Our adopted S-factors are listed in Table 7.

### A.4. *The $^3$He(d,p)$^4$He and d($^3$He,p)$^4$He data of Geist et al. (1999)*

The cross section data are presented in Figure 5 of Geist et al. (1999) and are available in tabular form from EXFOR, as communicated by the authors. Three data sets exist, one for the $^3$He(d,p)$^4$He reaction and two for the d($^3$He,p)$^4$He reaction. The data are listed in Table 8, with statistical uncertainties only. We do not distinguish between the $^3$He(d,p)$^4$He and d($^3$He,p)$^4$He reactions because all data points were measured at center-of-mass energies above 50 keV where electron screening effects can be disregarded. A systematic uncertainty of 4.3% is obtained by adding quadratically the contributions from the d(d,p)$^3$H monitor cross section scale and fitting procedure (1.3% and 3%, respectively), the incident beam energy and energy loss (2%), and the beam integration (2%).

### A.5. *The d($^3$He,p)$^4$He data of Costantini et al. (2000)*

We adopted the d($^3$He,p)$^4$He results of Table 1 in Costantini et al. (2000), which lists the effective energy, Sfactor, statistical uncertainty, and systematic uncertainty. The latter ranges from 8% at the lowest energy (4.22 keV) to 3.0% at the highest energy (13.83 keV). In our analysis, we assume an average systematic uncertainty of 5.5%. Table 9 lists the S-factors adopted in the present work.

### A.6. *The $^3$He(d,p)$^4$He and d($^3$He,p)$^4$He data of Aliotta et al. (2001)*

The S-factor data for the $^3$He(d,p)$^4$He and d($^3$He,p)$^4$He reactions are taken from Tables 1 and 2, respectively, in Aliotta et al. (2001). The quoted uncertainties include only statistical (2.6%) effects. The systematic uncertainty arises from the target pressure, calorimeter, and detection efficiency, and amounts to 3.0%. The S-factor data adopted in the present work are listed in Table 10.

### A.7. *Other data*

The following data sets were excluded from our analysis. Bonner et al. (1952) only present differential cross sections measured at zero degrees. The cross section data of Jarvis & Roaf (1953), obtained using photographic plates, are presented in their Table 1 for three bombarding energies. However, the origin of their quoted errors (6% − 14%) is

**Table 7.** The d($^3$He,p)$^4$He data of Möller & Besenbacher (1980).

| $E_{c.m.}$ (MeV) | $S$ (MeVb) | $\Delta S_{\rm stat}$ (MeVb) | $\Delta S_{\rm sys}$ (MeVb) |
|---|---|---|---|
| 0.0856 | 7.17 | 0.50 | 0.28 |
| 0.1460 | 14.18 | 0.42 | 0.55 |
| 0.1736 | 16.68 | 0.50 | 0.65 |
| 0.2056 | 18.58 | 0.56 | 0.72 |
| 0.2196 | 17.24 | 0.52 | 0.67 |
| 0.2336 | 17.65 | 0.53 | 0.69 |
| 0.2668 | 14.77 | 0.44 | 0.58 |
| 0.2964 | 13.22 | 0.40 | 0.52 |
| 0.3088 | 11.22 | 0.34 | 0.44 |
| 0.3280 | 10.16 | 0.30 | 0.40 |
| 0.3856 | 7.34 | 0.22 | 0.29 |
| 0.4460 | 5.02 | 0.15 | 0.20 |
| 0.5064 | 3.87 | 0.12 | 0.15 |
| 0.5648 | 2.885 | 0.086 | 0.11 |
| 0.6256 | 2.337 | 0.070 | 0.090 |
| 0.6836 | 2.011 | 0.060 | 0.080 |
| 0.7504 | 1.681 | 0.050 | 0.070 |
| 0.8068 | 1.553 | 0.046 | 0.060 |

not clear. Yarnell et al. (1953) report the differential cross section at 86° (see their Figure 6), but the bombarding energy uncertainty is large (3% − 14%) and the different contributions to the total cross section uncertainty cannot be estimated individually from the information provided. The latter argument also holds for the data of Freier & Holmgren (1954) (see their Figure 1). Arnold et al. (1954) provide cross sections between 36 keV and 93 keV bombarding deuteron energy (see their Table 3), including a detailed error analysis. However it was suggested by Coc et al. (2015) that an unaccounted systematic error affected the d(d,n)$^3$He cross section measured in the same experiment. For the data of Kunz (1955), we could not estimate separately the statistical and systematic uncertainty contributions. We disregarded the data of La Cognata et al. (2005) because their indirect method does not provide absolute cross section values. They normalized their results to cross sections obtained in other experiments, mainly the data of Geist et al. (1999). See also the discussion in Barker (2007) regarding the absolute cross section normalization of La Cognata et al. (2005). We did not include the data of Engstler et al. (1988) and Prati et al. (1994) in our analysis because these results are biased by stopping-power problems. Finally, we also did not take into account the results of Barbui et al. (2013), who reported the plasma$^3$He(d,p)$^4$He S-factor using intense ultrafast laser pulses. The derivation of the S-factor versus center of mass energy from the measured Maxwellian-averaged cross section at different plasma temperatures is complicated and the systematic effects are not obvious to us.

**Table 8.** The $^3$He(d,p)$^4$He and d($^3$He,p)$^4$He data of Geist et al. (1999).

| $E_{c.m.}$ (MeV) | $S \pm \Delta S_{\rm stat}$[a] (MeVb) | $E_{c.m.}$ (MeV) | $S \pm \Delta S_{\rm stat}$[a] (MeVb) |
|---|---|---|---|
| 0.1527 | 15.89±0.11 | 0.3344 | 8.965±0.033 |
| 0.1645 | 16.76±0.21 | 0.3463 | 8.273±0.046 |
| 0.1762 | 17.07±0.14 | 0.3583 | 7.640±0.041 |
| 0.1880 | 17.36±0.20 | 0.3702 | 7.134±0.045 |
| 0.1899 | 17.418±0.067 | 0.3821 | 6.571±0.037 |
| 0.1999 | 17.40±0.15 | 0.3880 | 6.309±0.036 |
| 0.2017 | 17.562±0.094 | 0.1468 | 14.64±0.22 |
| 0.2117 | 17.38±0.23 | 0.1702 | 16.94±0.23 |
| 0.2236 | 16.36±0.21 | 0.1779 | 16.64±0.23 |
| 0.2255 | 16.635±0.070 | 0.2092 | 17.02±0.22 |
| 0.2374 | 15.86±0.12 | 0.2170 | 17.02±0.22 |
| 0.2493 | 15.08±0.12 | 0.2404 | 15.79±0.21 |
| 0.2612 | 14.12±0.10 | 0.2522 | 14.903±0.081 |
| 0.2732 | 13.300±0.045 | 0.2542 | 14.747±0.059 |
| 0.2746 | 13.399±0.052 | 0.2717 | 13.27±0.11 |
| 0.2851 | 12.181±0.077 | 0.2855 | 12.68±0.11 |
| 0.2866 | 12.464±0.083 | 0.3029 | 10.69±0.14 |
| 0.2971 | 11.520±0.079 | 0.3169 | 10.17±0.11 |
| 0.2985 | 11.428±0.064 | 0.3482 | 8.012±0.083 |
| 0.3089 | 10.474±0.090 | 0.3795 | 6.394±0.074 |
| 0.3105 | 10.598±0.055 | 0.4108 | 5.351±0.060 |
| 0.3224 | 9.6450±0.053 | | |

[a] Systematic uncertainty: 4.3%.

**Table 9.** The d($^3$He,p)$^4$He data of Costantini et al. (2000).

| $E_{c.m.}$ (MeV) | $S \pm \Delta S_{\rm stat}$[a] (MeVb) | $E_{c.m.}$ (MeV) | $S \pm \Delta S_{\rm stat}$[a] (MeVb) |
|---|---|---|---|
| 0.00422 | 9.7±1.7 | 0.00834 | 7.51±0.22 |
| 0.00459 | 9.00±0.67 | 0.00851 | 7.38±0.22 |
| 0.00471 | 8.09±0.62 | 0.00860 | 7.65±0.23 |
| 0.00500 | 8.95±0.70 | 0.00871 | 7.82±0.28 |
| 0.00509 | 9.8±1.0 | 0.00898 | 7.36±0.19 |
| 0.00537 | 8.86±0.48 | 0.00908 | 7.66±0.17 |
| 0.00544 | 8.01±0.39 | 0.00914 | 7.60±0.24 |
| 0.00551 | 9.68±0.70 | 0.00929 | 7.54±0.23 |
| 0.00554 | 8.87±0.55 | 0.00938 | 7.47±0.14 |
| 0.00577 | 8.99±0.31 | 0.00948 | 7.59±0.13 |
| 0.00583 | 8.93±0.36 | 0.00978 | 7.32±0.22 |
| 0.00590 | 8.74±0.25 | 0.00987 | 7.52±0.19 |
| 0.00593 | 8.31±0.55 | 0.00991 | 7.24±0.18 |
| 0.00623 | 8.15±0.29 | 0.01007 | 7.39±0.19 |
| 0.00631 | 8.10±0.23 | 0.01018 | 7.35±0.14 |
| 0.00652 | 8.26±0.48 | 0.01029 | 7.44±0.17 |
| 0.00657 | 8.03±0.26 | 0.01087 | 7.38±0.16 |
| 0.00672 | 8.32±0.16 | 0.01096 | 7.35±0.13 |
| 0.00700 | 7.90±0.27 | 0.01105 | 7.41±0.17 |
| 0.00707 | 8.32±0.28 | 0.01165 | 7.24±0.14 |
| 0.00734 | 7.70±0.16 | 0.01178 | 7.21±0.12 |
| 0.00740 | 7.69±0.15 | 0.01185 | 7.35±0.11 |
| 0.00746 | 7.90±0.18 | 0.01241 | 7.58±0.14 |
| 0.00752 | 7.83±0.26 | 0.01255 | 7.31±0.13 |
| 0.00812 | 7.31±0.11 | 0.01265 | 7.31±0.14 |
| 0.00819 | 7.31±0.25 | 0.01307 | 7.36±0.13 |
| 0.00822 | 7.43±0.24 | 0.01383 | 7.23±0.13 |
| 0.00829 | 7.85±0.24 | | |

[a] Average systematic uncertainty: 5.5%.

**Table 10.** The $^3$He(d,p)$^4$He and d($^3$He,p)$^4$He data of Aliotta et al. (2001)[a].

| $E_{c.m.}$ (MeV) | $S \pm \Delta S_{\rm stat}$[c] (MeVb) | $E_{c.m.}$ (MeV) | $S \pm \Delta S_{\rm stat}$[c] (MeVb) |
|---|---|---|---|
| 0.00501 | 10.8±1.5 | 0.02508 | 7.18±0.20 |
| 0.00550 | 10.31±0.81 | 0.02592[b] | 7.17±0.19 |
| 0.00601 | 9.41±0.48 | 0.02662 | 6.93±0.18 |
| 0.00602 | 10.37±0.35 | 0.02788[b] | 7.01±0.19 |
| 0.00645 | 9.36±0.35 | 0.02873 | 7.22±0.20 |
| 0.00690 | 8.82±0.31 | 0.02988[b] | 7.19±0.19 |
| 0.00751 | 9.12±0.29 | 0.02991 | 6.87±0.18 |
| 0.00780 | 8.66±0.28 | 0.03110 | 7.24±0.20 |
| 0.00818 | 8.31±0.24 | 0.03190[b] | 7.17±0.19 |
| 0.00896 | 7.85±0.26 | 0.03289 | 7.04±0.20 |
| 0.00902 | 7.88±0.22 | 0.03349 | 7.33±0.20 |
| 0.00966 | 7.68±0.22 | 0.03389[b] | 7.43±0.20 |
| 0.01072 | 7.48±0.20 | 0.03586 | 7.22±0.18 |
| 0.01144 | 7.29±0.20 | 0.03589[b] | 7.39±0.19 |
| 0.01195[b] | 7.19±0.35 | 0.03589[b] | 7.58±0.20 |
| 0.01199 | 7.35±0.20 | 0.03788[b] | 7.63±0.20 |
| 0.01318 | 7.28±0.20 | 0.03858 | 7.33±0.18 |
| 0.01395[b] | 6.95±0.23 | 0.03987[b] | 7.65±0.20 |
| 0.01439 | 7.04±0.20 | 0.04067 | 7.44±0.22 |
| 0.01499 | 7.07±0.20 | 0.04187 | 7.29±0.20 |
| 0.01595[b] | 6.87±0.18 | 0.04306 | 7.48±0.22 |
| 0.01675 | 7.16±0.20 | 0.04485 | 7.40±0.20 |
| 0.01794[b] | 6.91±0.19 | 0.04544 | 7.70±0.22 |
| 0.01799 | 7.02±0.20 | 0.04786 | 7.63±0.20 |
| 0.01914 | 7.20±0.20 | 0.05021 | 7.66±0.22 |
| 0.01993[b] | 6.75±0.18 | 0.05083 | 7.70±0.20 |
| 0.02094 | 6.81±0.18 | 0.05265 | 7.70±0.22 |
| 0.02155 | 7.09±0.20 | 0.05382 | 7.77±0.22 |
| 0.02192[b] | 6.96±0.19 | 0.05504 | 7.77±0.22 |
| 0.02271 | 7.13±0.20 | 0.05681 | 7.88±0.20 |
| 0.02392[b] | 6.92±0.19 | 0.05741 | 7.94±0.22 |
| 0.02393 | 6.91±0.18 | 0.05980 | 8.12±0.22 |

[a] S-factors obtained from $^3$He(d,p)$^4$He measurement, unless noted otherwise.

[b] S-factors obtained from d($^3$He,p)$^4$He measurement.

[c] Systematic uncertainty: 3.0%.

## REFERENCES


Aliotta, M., Raiola, F., Gyrky, G., et al. 2001, Nuclear Physics A, 690, 790 . http://www.sciencedirect.com/science/article/pii/S0375947401003669

Arnold, W. R., Phillips, J. A., Sawyer, G. A., Stovall, E. J., & Tuck, J. L. 1954, Phys. Rev., 93, 483. https://link.aps.org/doi/10.1103/PhysRev.93.483

Assenbaum, H. J., Langanke, K., & Rolfs, C. 1987, Zeitschrift für Physik A Atomic Nuclei, 327, 461. https://doi.org/10.1007/BF01289572

Aver, E., Olive, K. A., & Skillman, E. D. 2015, JCAP, 7, 011

Bania, T. M., Rood, R. T., & Balser, D. S. 2002, Nature, 415, 54

Barbui, M., Bang, W., Bonasera, A., et al. 2013, Phys. Rev. Lett., 111, 082502. https://link.aps.org/doi/10.1103/PhysRevLett.111.082502

Barker, F. 2002, Nuclear Physics A, 707, 277 . http://www.sciencedirect.com/science/article/pii/S0375947402009211

Barker, F. C. 1997, Phys. Rev. C, 56, 2646. https://link.aps.org/doi/10.1103/PhysRevC.56.2646

—. 2007, Phys. Rev. C, 75, 027601. https://link.aps.org/doi/10.1103/PhysRevC.75.027601

Bonner, T. W., Conner, J. P., & Lillie, A. B. 1952, Phys. Rev., 88, 473. https://link.aps.org/doi/10.1103/PhysRev.88.473

Coc, A., Descouvemont, P., Olive, K. A., Uzan, J.-P., & Vangioni, E. 2012, Phys. Rev. D, 86, 043529. https://link.aps.org/doi/10.1103/PhysRevD.86.043529

Coc, A., Petitjean, P., Uzan, J.-P., et al. 2015, Phys. Rev. D, 92, 123526. https://link.aps.org/doi/10.1103/PhysRevD.92.123526

Coc, A., & Vangioni, E. 2010, Journal of Physics: Conference Series, 202, 012001. http://stacks.iop.org/1742-6596/202/i=1/a=012001

Cooke, R. J. 2015, The Astrophysical Journal Letters, 812, L12. http://stacks.iop.org/2041-8205/812/i=1/a=L12

Cooke, R. J., Pettini, M., Jorgenson, R. A., Murphy, M. T., & Steidel, C. C. 2014, ApJ, 781, 31

Costantini, H., Formicola, A., Junker, M., et al. 2000, Physics Letters B, 482, 43 . http://www.sciencedirect.com/science/article/pii/S037026930000513X

Cyburt, R. H., Fields, B. D., Olive, K. A., & Yeh, T.-H. 2016, Rev. Mod. Phys., 88, 015004. https://link.aps.org/doi/10.1103/RevModPhys.88.015004

de Souza, R. S., Hilbe, J. M., Buelens, B., et al. 2015, MNRAS, 453, 1928

de Souza, R. S., Dantas, M. L. L., Krone-Martins, A., et al. 2016, MNRAS, 461, 2115

Descouvemont, P., Adahchour, A., Angulo, C., Coc, A., & Vangioni-Flam, E. 2004, Atomic Data and Nuclear Data Tables, 88, 203

Descouvemont, P., & Baye, D. 2010, Reports on Progress in Physics, 73, 036301

Engstler, S., Krauss, A., Neldner, K., et al. 1988, Physics Letters B, 202, 179 . http://www.sciencedirect.com/science/article/pii/0370269388900032

EXFOR. 2017. http://www.nndc.bnl.gov/exfor/exfor.htm

Freier, G., & Holmgren, H. 1954, Physical Review, 93, 825

Gamow, G. 1948, Nature, 162, 680

Geist, W. H., Brune, C. R., Karwowski, H. J., et al. 1999, Phys. Rev. C, 60, 054003. https://link.aps.org/doi/10.1103/PhysRevC.60.054003

Gómez Iñesta, A., Iliadis, C., & Coc, A. 2017, The Astrophysical Journal, 849, 134. http://stacks.iop.org/0004-637X/849/i=2/a=134

Heinrich, J., & Lyons, L. 2007, Annual Review of Nuclear and Particle Science, 57, 145. https://doi.org/10.1146/annurev.nucl.57.090506.123052

Hilbe, J. M., de Souza, R. S., & Ishida, E. E. O. 2017, Bayesian Models for Astrophysical Data Using R, JAGS, Python, and Stan, doi:10.1017/CBO9781316459515

Iliadis, C., Anderson, K. S., Coc, A., Timmes, F. X., & Starrfield, S. 2016, The Astrophysical Journal, 831, 107. http://stacks.iop.org/0004-637X/831/i=1/a=107

Jarvis, R., & Roaf, D. 1953, Proceedings of the Royal Society of London A: Mathematical, Physical and Engineering Sciences, 218, 432. http://rspa.royalsocietypublishing.org/content/218/1134/432

Jaynes, E., & Bretthorst, G. 2003, Probability Theory: The Logic of Science (Cambridge University Press). https://books.google.com/books?id=tTN4HuUNXjgC

Krauss, A., Becker, H., Trautvetter, H., Rolfs, C., & Brand, K. 1987, Nuclear Physics A, 465, 150 . http://www.sciencedirect.com/science/article/pii/0375947487903022

Kunz, W. E. 1955, Physical Review, 97, 456

La Cognata, M., Spitaleri, C., Tumino, A., et al. 2005, Phys. Rev. C, 72, 065802. https://link.aps.org/doi/10.1103/PhysRevC.72.065802

Lane, A. M., & Thomas, R. G. 1958, Rev. Mod. Phys., 30, 257. https://link.aps.org/doi/10.1103/RevModPhys.30.257

Lane, A. M., & Thomas, R. G. 1958, Rev. Mod. Phys., 30, 257. https://link.aps.org/doi/10.1103/RevModPhys.30.257

Möller, W., & Besenbacher, F. 1980, Nuclear Instruments and Methods, 168, 111

Parent, E., & Rivot, E. 2012, Introduction to Hierarchical Bayesian Modeling for Ecological Data, Chapman & Hall/CRC Applied Environmental Statistics (Taylor & Francis). https://books.google.com/books?id=YYt-ZUTvbjUC

Peebles, P. J., & Ratra, B. 2003, Reviews of Modern Physics, 75, 559

Planck Collaboration, Adam, R., Ade, P. A. R., et al. 2016, A&A, 594, A1

Plummer, M. 2003, in Proceedings of the 3rd International Workshop on Distributed Statistical Computing

Prati, P., Arpesella, C., Bartolucci, F., et al. 1994, Zeitschrift für Physik A Hadrons and Nuclei, 350, 171. https://doi.org/10.1007/BF01290685

Riess, A. G., Filippenko, A. V., Challis, P., et al. 1998, AJ, 116, 1009

Sallaska, A. L., Iliadis, C., Champange, A. E., et al. 2013, ApJS, 207, 18

Savage, M. J., Scaldeferri, K. A., & Wise, M. B. 1999, Nuclear Physics A, 652, 273

Sbordone, L., Bonifacio, P., Caffau, E., et al. 2010, A&A, 522, A26. https://doi.org/10.1051/0004-6361/200913282

Spergel, D. N., Bean, R., Doré, O., et al. 2007, ApJS, 170, 377

Team, R. D. C. 2010, R: A language and environment for statistical computing, R Foundation for Statistical Computing, Vienna, Austria. http://www.r-project.org

Trotta, R. 2017, arXiv:1701.01467, arXiv:1701.01467

Wigner, E. P., & Eisenbud, L. 1947, Physical Review, 72, 29

Woods, C. L., Barker, F. C., Catford, W. N., Fifield, L. K., & Orr, N. A. 1988, Australian Journal of Physics, 41, 525

Yarnell, J. L., Lovberg, R. H., & Stratton, W. R. 1953, Physical Review, 90, 292

Zhichang, L., Jingang, Y., & Xunliang, D. 1977, Atom. Ener. Sci. Tech., 129